Supporting Information for

Self-powered electrochemical synthesis of hydrogen peroxide from air and lignin

Yongrong Li [a, b, #], Denghao Ouyang [a, b,#], Xi Liu [a, b], Yichen Zhang [a, b], Zhiqiang Niu [c], J.Y. Zhu [d], Xuejun Pan [e], Xuebing Zhao [a, b,*]

[a] *Key Laboratory of Industrial Biocatalysis, Ministry of Education, Tsinghua University, Beijing 100084, China;*

[b] *Institute of Applied Chemistry, Department of Chemical Engineering, Tsinghua University, Beijing 100084, China;*

[c] *State Key Laboratory of Chemical Engineering, Department of Chemical Engineering, Tsinghua University, Beijing 100084,China;*

[d] *Forest Products Laboratory, U.S. Department of Agriculture, Forest Service, Madison, Wisconsin 53726, United States;*

[e] *Department of Biological Systems Engineering, University of Wisconsin-Madison, Madison, Wisconsin 53706, United States.*

[#] These authors contributed equally to this work.

***Corresponding author:**

Xuebing Zhao, Email: zhaoxb@mail.tsinghua.edu.cn (X. Zhao)

1. Experimental section

1.1 Chemicals and materials

The chemical reagents used in the experiments were analytical grade and used without further purification, including sodium lignosulfonate, boric acid (H_3BO_3), nano-silica (SiO_2), potassium hydroxide (KOH), potassium ferricyanide ($K_3[Fe(CN)_6]$), sulfuric acid (H_2SO_4), hydrochloric acid (HCl), carbon paper with hydrophobic treatment of one-side by polytetrafluoroethylene (PTFE), ammonium metavanadate (NH_4VO_3), and 5-hydroxymethylfurfural (HMF). Nafion 115 proton exchange membrane was manufactured by DuPont Company (DE, USA). Prior to use, the Nafion 115 membrane was activated by a standard procedure.[1]

1.2 Preparation of B, O doped carbon-based catalysts

B, O doped carbon-based catalysts (B,O-C) were synthesized via the pyrolysis of a mixture of H_3BO_3, SiO_2, and sodium lignosulfonate (Fig. 2a). In optimized proportional conditions, 2 g H_3BO_3, 1 g SiO_2, and 1 g sodium lignosulfonate were dispersed in 50 mL deionized water. Then the slurry was freeze-dried to obtain a homogeneous precursor powder. Subsequently, the obtained powder was heated in a tube furnace at 700 ℃, 900 ℃, and 1100 ℃, respectively, for 2 h at a heating rate of 5 ℃ min^{-1} under nitrogen atmosphere. The carbonized powder was then dispersed in a 5 M KOH solution for 12 h under magnetic stirring to remove the SiO_2. Furthermore, the sample was thoroughly washed with deionized water and then dried at 60 ℃ for 12 h. The dried catalysts were directly used without further modification. The B,O-C catalysts prepared by pyrolysis at 700 ℃, 900 ℃, and 1100 ℃ were named B,O-C-700, B,O-C-900 and B,O-C-1100, respectively.

1.3 Characterization of B, O doped carbon-based catalysts

The surface morphology and elemental analysis of the prepared catalysts were analyzed with a scanning electron microscope (SEM) equipped with an energy dispersive spectrometer (EDS) (Hitachi S-3400 N II, Hitachi, Japan). The X-ray diffusion (XRD) analysis was conducted using a D/Max 2500H (Rigaku, Japan) diffractometer. The X-ray photoelectron spectroscopy (XPS) was recorded using a

Thermo Fisher ESCALAB 250 Xi X-ray photoelectron spectrometer (Thermo Fisher, MA, USA). Raman spectra were collected at 532 nm on a HR800 Raman spectrometer (HORIBA, French). FTIR spectra were recorded using an IRTracer-100 (Shimadzu, Japan). The mesopore and macropore properties of the prepared catalysts were analyzed using nitrogen adsorption-desorption tests with a SI-MP instrument (Quantachrome, USA).

1.4 Electrochemical measurements

The properties of the prepared catalysts for H_2O_2 production were firstly analyzed using a typical three-electrode system with a rotating ring-disk electrode (RRDE) as a working electrode, a saturated calomel electrode (SCE) electrode as a reference electrode, and a Pt mesh electrode as a counter electrode by a CHI-760E electrochemical workstation (Chenhua, China). The rotation rate was maintained at 1600 rpm to ensure the formed H_2O_2 diffusion to the Pt ring while minimizing the H_2O_2 decomposition. The electrolyte was a 0.1 M KOH solution (pH = 13) saturated by nitrogen or oxygen. The catalyst ink was prepared with 3.3 mg catalyst, 1 mL anhydrous ethanol, and 10 μL Nafion (5 wt%), and then sonicated for 20 min. Then, 8 μL of the ink was carefully dropped on the disk electrode in RRDE to obtain a uniform ink layer with a rough mass loading of 0.2 mg cm^{-2} and then dried naturally. Liner sweep voltammetry (LSV) curves were recorded at 10 mV s^{-1} and 1600 rpm with 100% internal resistance (iR) compensation. According to the Nernst equation, all potentials measured against SCE could be converted to the reversible hydrogen electrode (RHE) scale with the following equation:

$$E_{\text{vs. }RHE} = E_{\text{vs. }SCE} + 0.059\text{pH} + 0.241 \quad (1)$$

The molar selectivity of H_2O_2 ($S_{H_2O_2}$) and the transferred electron number (n) were calculated by the following equation[2]:

$$S_{H_2O_2}(\%) = 200 \times \frac{I_r}{\frac{I_r}{N} + I_d} \times 100\% \quad (2)$$

$$n = 4\frac{I_d}{\frac{I_r}{N} + I_d} \quad (3)$$

where I_d is the disk current (or the current caused by the oxygen reduction reaction) and I_r is the ring current (or the current caused by the H_2O_2 oxidation); N is the current collection efficiency, which was measured as 0.37. To completely oxidize H_2O_2, a high potential of 1.2 V vs. RHE was applied to the Pt ring.

1.5 Electrosynthesis of H_2O_2

Electrosynthesis of H_2O_2 was conducted in both an H-type cell and a flow cell at a constant potential (voltage) or current with or without iR compensation. Catalyst ink was prepared by dispersing 8 mg of the prepared catalyst in 3 mL anhydrous ethanol, followed by adding 20 μL 60 wt% PTFE solution. The ink mixture was sonicated for 20 min and then evenly sprayed onto the non-hydrophobic side of the carbon paper (6 cm^2) and dried under an infrared lamp. The catalyst loading on the carbon paper was estimated as 1 mg cm^{-2} based on the mass difference of the carbon paper matrix before and after spraying. H-type cell test was carried out in a two-chamber glass electrolyzer using a typical three-electrode system with the catalyst-loaded carbon paper as a working electrode, SCE electrode as a reference electrode, and Pt mesh as a counter electrode. A Nafion 115 membrane was used as a separator, while a KOH solution (0.1 M or 1 M) was used as the electrolyte at both anode and cathode side. Air (oxygen) was continuously bubbled into the catholyte during the electrolysis test. The area of the carbon paper immersed in the electrolyte was 1 cm^2, and the volume of the catholyte was 50 mL. The flow cell test was carried out in a three-chamber flow cell system (Fig. 6b) developed in our lab with carbon paper as a self-breathing cathode and NiFe-LDH@Ni foam or commercial Ru-Ir/Ti mesh as an anode. The carbon paper loaded with the prepared catalysts was sandwiched between the gas chamber and the catholyte chamber. The side coated with catalysts was exposed to the catholyte, while the hydrophobically-treated side was exposed to air. This hydrophobic carbon paper could efficiently prevent the leakage of the electrolyte but allow the gas diffusing across the paper to contact the catalysts. Moreover, the Nafion 115 membrane was further

sandwiched in the anolyte chamber and catholyte chamber to separate the electrolyte. 1 M KOH solution was continuously circulated in the cathode and anode chambers, respectively, by peristaltic pumps, while fresh air was continuously ventilated into the gas chamber at a flow rate of 1.2 mL s^{-1}. The active area of the cathode was about 3 cm^2. For the paired system, a solution containing 0.25 M $K_3[Fe(CN)_6]$, 1 M KOH, and 8 g L^{-1} alkali lignin was used as the anolyte ,Ni foam was used as an anode, and the cathode was the same as unpaired system.

Direct lignin fuel cell (DLFC) developed in our previous work[3] was used as a power source to drive the electrolytic cell. The structure of DLFC and the electron transport chain are schematically shown in Fig. S10. The DLFC employed $Fe(CN)_6^{3-}$ /$Fe(CN)_6^{4-}$ and VO_2^+/VO^{2+}as the electron mediators in anolyte for lignin oxidation and catholyte for the oxygen reduction reaction, respectively. The cell consisted of two graphite plates with flow channels in a 2 cm × 2 cm area as the anode and cathode, respectively, and corresponding copper sheets as current collectors. Ion exchange membrane such as proton exchange membrane (Nafion 115) was used to separate the anode and cathode chambers. Two DLFCs were used in series with a total area of 8 cm^2 to provide enough voltage for the electrolytic cell.

H_2O_2 concentration was detected by the ultraviolet-visible spectrophotometer (UV-1800, Shimadzu, Japan) with NH_4VO_3 colorimetric method[4]. Typically, 100 μL catholyte, 400 μL 2 M H_2SO_4, and 1 mL 2 g L^{-1} NH_4VO_3 solution were added into a 5-mL volumetric flask. Deionized water was then added to match the scale line. After 5 min, the absorbance of the solution at 453 nm was measured. Then the H_2O_2 concentration was calculated based on a prepared standard curve.

1.6 In-situ ATR-IR test

Surface enhanced infrared absorption spectroscopy (SEIRAS) with attenuated total reflection (ATR) configuration was employed to study the catalytic mechanism of the prepared catalysts. A Thermo Nicolet 8700 spectrometer equipped with an MCT detector cooled by liquid nitrogen was employed for the electrochemical ATR-SEIRAS measurements. Chemical deposition of Au thin film (~60 nm) on the Si prism was

prepared as follows. Before the chemical deposition of Au, the Si prism surface for IR reflection was polished with diamond suspension and cleaned in water with sonication. Then the prism was soaked in a piranha solution (7:3 volumetric ratio of 98% H_2SO_4 to 30% H_2O_2) for 2 h to etch the surface and generate a hydrophobic surface. The plating solution prepared according to previously reported work[5] was quickly injected onto the Si surface which was pre-heated to 60 ℃. After 90 s, the plated surface was washed with water and dried by Ar gas, yielding an as-freshly deposited (AFD) Au film. 30 μL catalyst ink was deposited and dried on the Au-film, then the ink-coated prism was assembled into a spectroelectrochemical cell as the working electrode with a Pt mesh (1 cm × 1 cm) as a counter electrode. Ag/AgCl was used as a reference electrode, which was introduced near the working electrode via a Luggin capillary. All spectra data were calibrated according to the following equation:

$$\frac{\Delta R}{R} = \frac{E_S - E_R}{E_R} \times 100\% \tag{4}$$

$$E_{\text{vs.}RHE} = E_{\text{vs.}Ag/AgCl} + 0.059\text{pH} + 0.198 \tag{5}$$

where E_S and E_R represent the spectra intensity of the sample and the reference, respectively.[6] The spectral resolution was 4 cm^{-1} for all the measurements if not otherwise mentioned.

1.7 DFT calculation

In the density functional theory (DFT) calculation, projector-augmented-wave method with the Perdew-Burke-Ernzerhof GGA function was applied. [7,8] The electronic convergence limit was set to 1×10^{-5} eV. Optimization of atomic coordinates was converged when the Hellmann-Feynman force was smaller than 1×10^{-2} eV $Å^{-1}$. The slabs consisting of C, O, and H were used. Intermediate of *OOH was placed on the top of the slab surface. The vacuum region was about 10 Å in height. The change of energy during the conversion of the intermediate was calculated using the computational hydrogen electrode method[9]. U_L was the limiting potential for the reaction. The charge was investigated using the Bader charge decomposition method[10]. The Gibbs free energy changes of intermediates were calculated with zero-point energy,

and entropy correction using the equation bellows[11]:

$$\Delta G^* = \Delta E^* + (\Delta ZPE - T\Delta S) \quad (6)$$

where *ZPE*, *T,* and *S* correspond to zero-point energy, temperature, and entropy, respectively, and * represents the reaction intermediate.

1.8 Product analysis in HMF in-situ oxidation

The concentrations of the organics were determined by high-performance liquid chromatography (HPLC, Shimadzu SPD-20A) with a wavelength of UV-Vis detector set at 265 nm. A 4.6×250 mm Spursil 5 μm C18 column was applied. The HPLC eluent consisted of 85% (v/v) deionized water and 15% (v/v) acetonitrile and was performed at a flow rate of 0.6 mL min^{-1} for 23 min (column temperature: 45 °C). The samples were prepared by diluting 200 μL electrolyte to 2 mL by deionized water. The conversion of HMF, yield of HMFCA and BHMF, and carbon balance were calculated by the following equations:

$$\text{HMF Conversion (\%)} = \frac{n_{\text{consumed HMF}}}{n_{\text{HMF input}}} \times 100\% \quad (7)$$

$$\text{Yield (\%)} = \frac{n_{\text{experimentally formed}}}{n_{\text{theoretically formed}}} \times 100\% \quad (8)$$

$$\text{Carbon balance (\%)} = \frac{n_{\text{all organics}}}{n_{\text{HMF input}}} \times 100\% \quad (9)$$

2. Supporting Figures and Tables

Fig. S1 Surface morphology of the carbon-based catalyst without using SiO_2 template. (a) and (b) SEM images. (c) EDS mapping images.

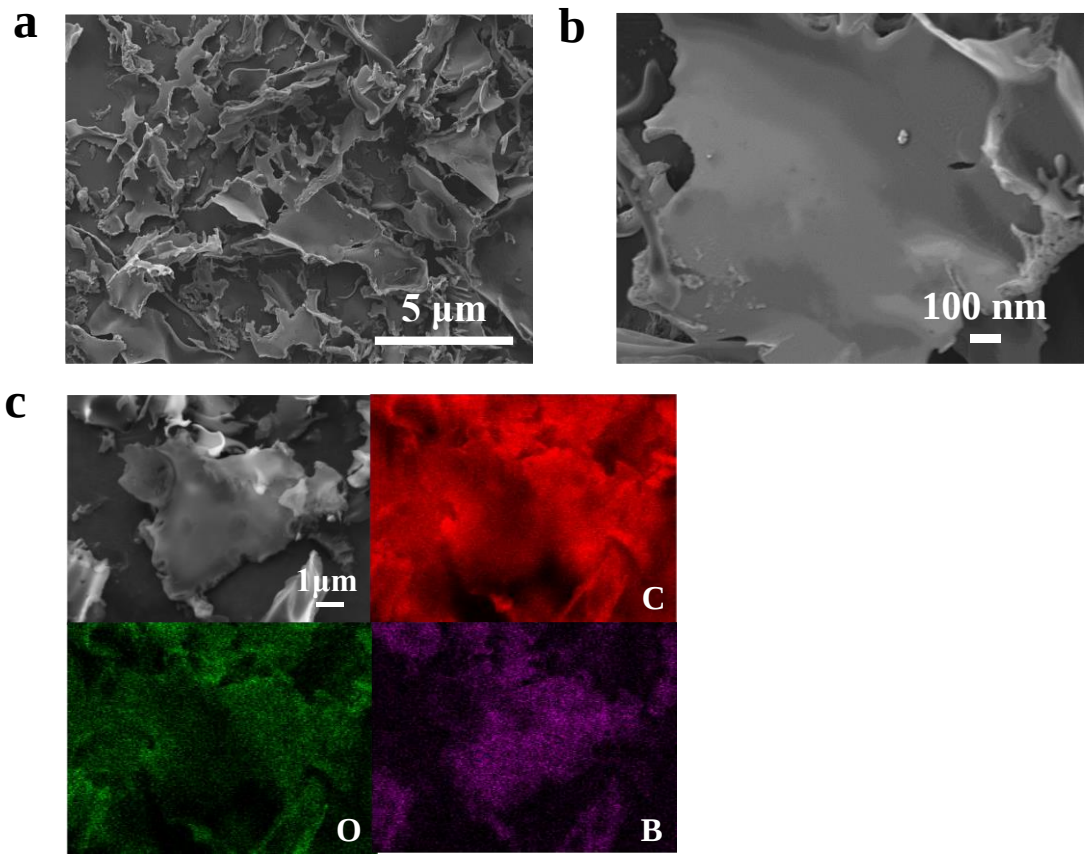

Fig. S2 TEM images of (a) B,O-C-700 and (b) B,O-C-1100.

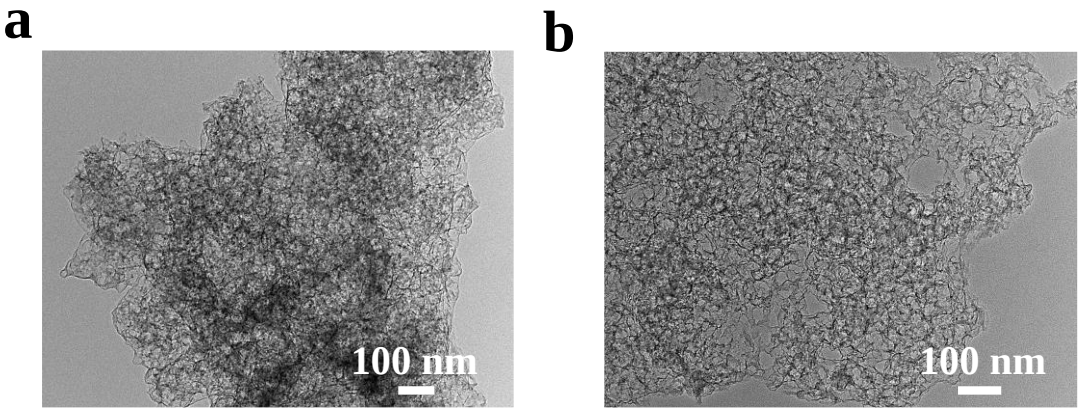

Fig. S3 Elemental and structural analysis of B,O-C-900. (a) High-resolution XPS spectra of Na1s. (b) FTIR spectrum.

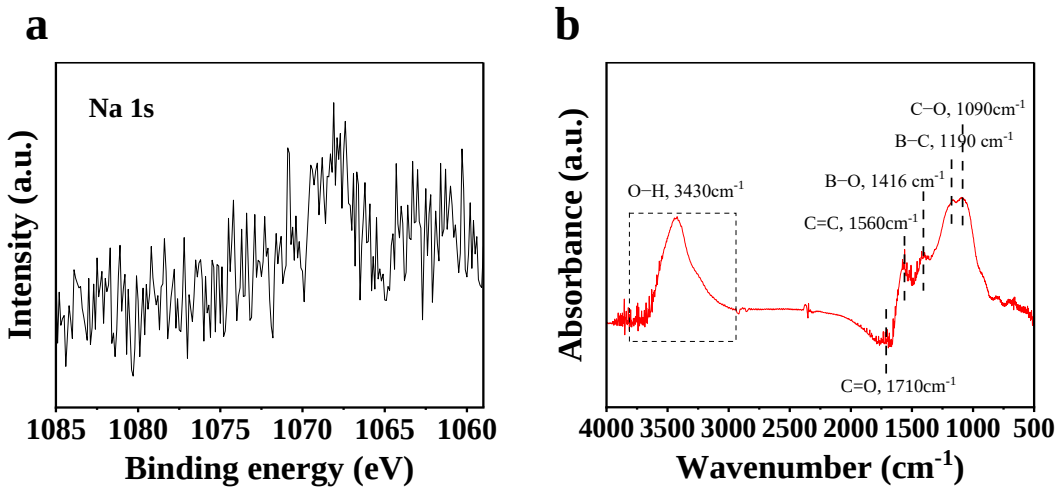

Fig. S4 Effects of addition of SiO_2 and H_3BO_3 on the electrochemical performance of carbon-based catalyst prepared by pyrolysis at 900 ℃. (a) LSV curves of the B,O-C-900 with different amount of SiO_2 template recorded in RRDE at a rotation rate of 1600 rpm in O_2-sturated 0.1M KOH and (b) the calculated H_2O_2 selectivity based on the corresponding LSV curves. (c) LSV curves of the B,O-C-900 with different amount of H_3BO_3 recorded in RRDE at a rotation rate of 1600 rpm in O_2-sturated 0.1M KOH and (d) the calculated H_2O_2 selectivity based on the corresponding LSV curves.

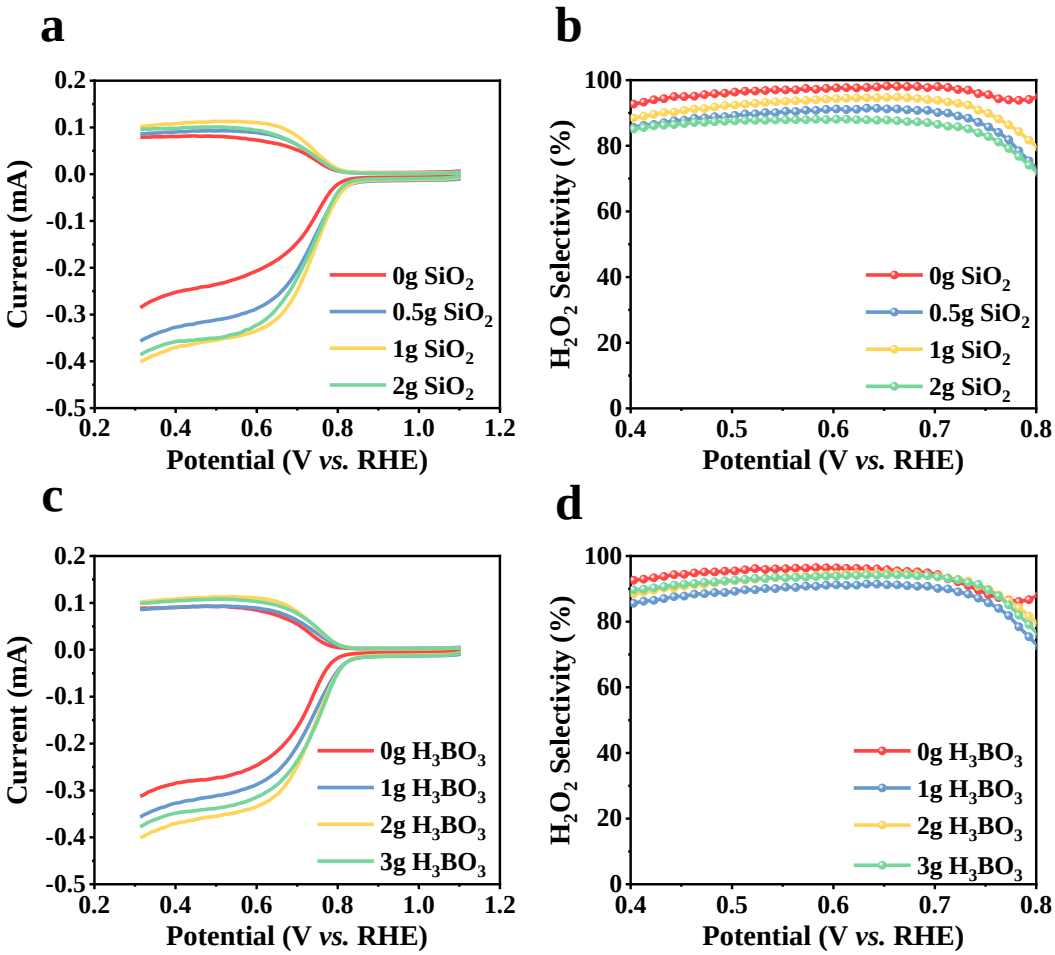

Fig. S5 The electrochemical performance of carbon-based catalysts prepared with different biomass derived organic precursors. (a) LSV curves of the B,O-C-900 with different precursors recorded in RRDE at a rotation rate of 1600 rpm in O_2-sturated 0.1 M KOH solution and (b) the calculated H_2O_2 selectivity based on the corresponding LSV curves. (c) H_2O_2 productivity and FE during electrolysis at 0.31V vs. RHE for 30 min in O_2-sturated 0.1M KOH.

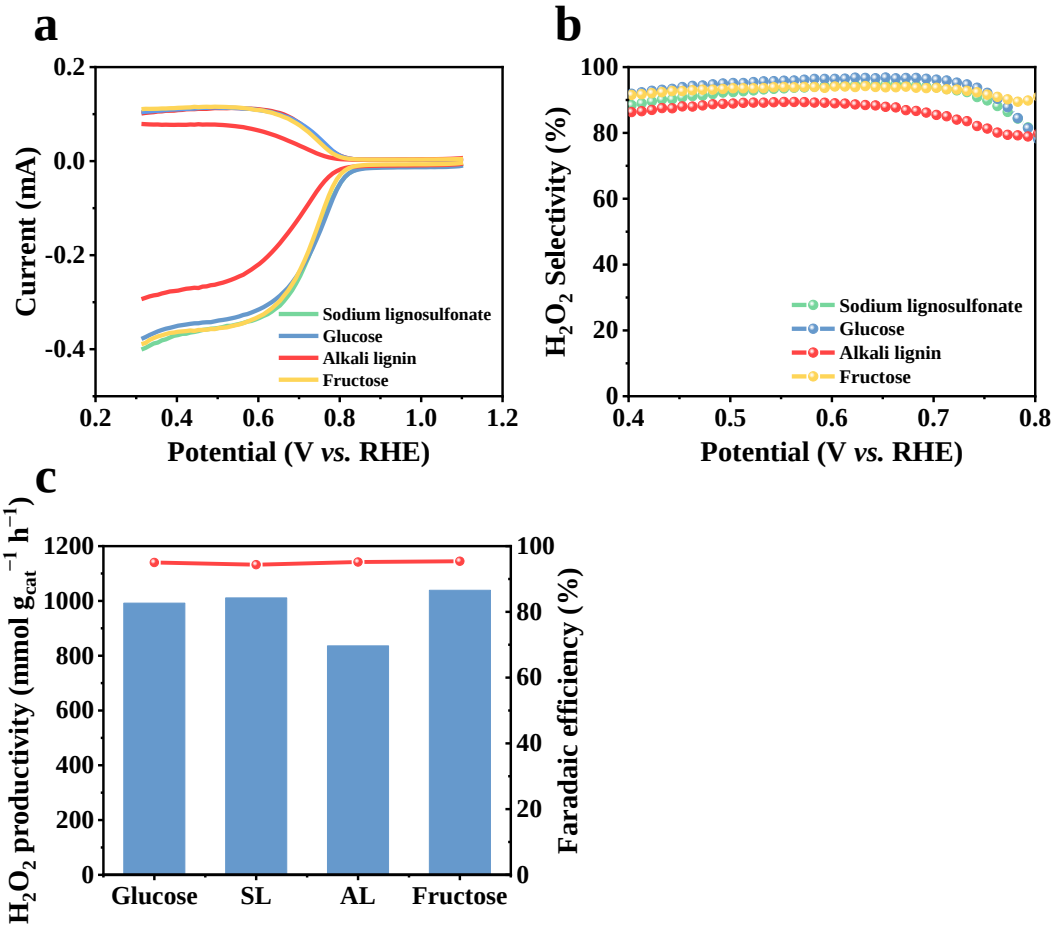

Fig. S6 Effects of iR compensation on the electrochemical performance of B,O-C-900. (a) LSV curves with different iR compensation. (b) Current density curves during electrolysis with different iR compensation at 0.51V vs. RHE for 30min in O_2-sturated KOH electrolyte.

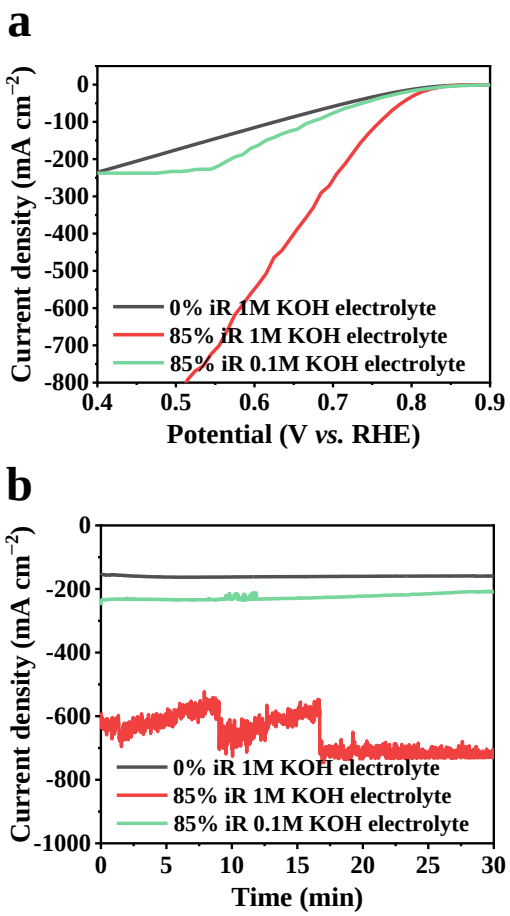

Fig. S7 Schematic diagrams of models for interaction between the active sites and O_2 used for theoretical calculations.

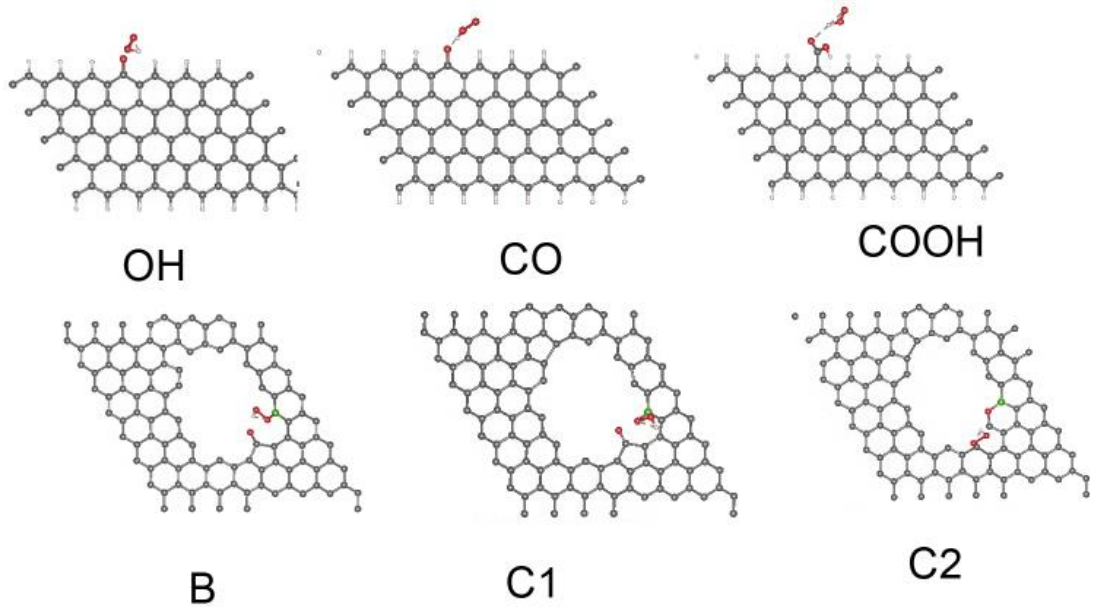

Fig. S8 Oxidation of lignin by $K_3[Fe(CN)_6]$ at room temperature. (a) Changes of reduction degree of $K_3[Fe(CN)_6]$ and the potential of the solution during the reaction of $K_3[Fe(CN)_6]$ with lignin. (b) Current density-time curves during electrolysis in a three-electrode system at 1.32V vs. RHE in 1 M KOH electrolyte containing 0.25 M $K_4[Fe(CN)_6]$ with or without lignin.

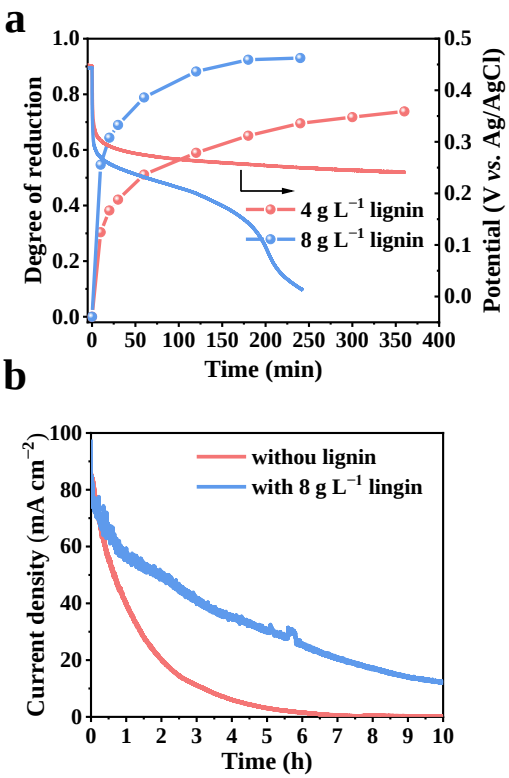

Fig. S9 Structure and electron transport chain of the direct lignin fuel cell used in this work. (a) Schematic diagram of the cell device. (b) Inherent electron transport chain constructed with $Fe(CN)_6^{3-}/Fe(CN)_6^{4-}$ as the anode electron mediators and VO_2^+/VO^{2+} as the cathode electron mediator.

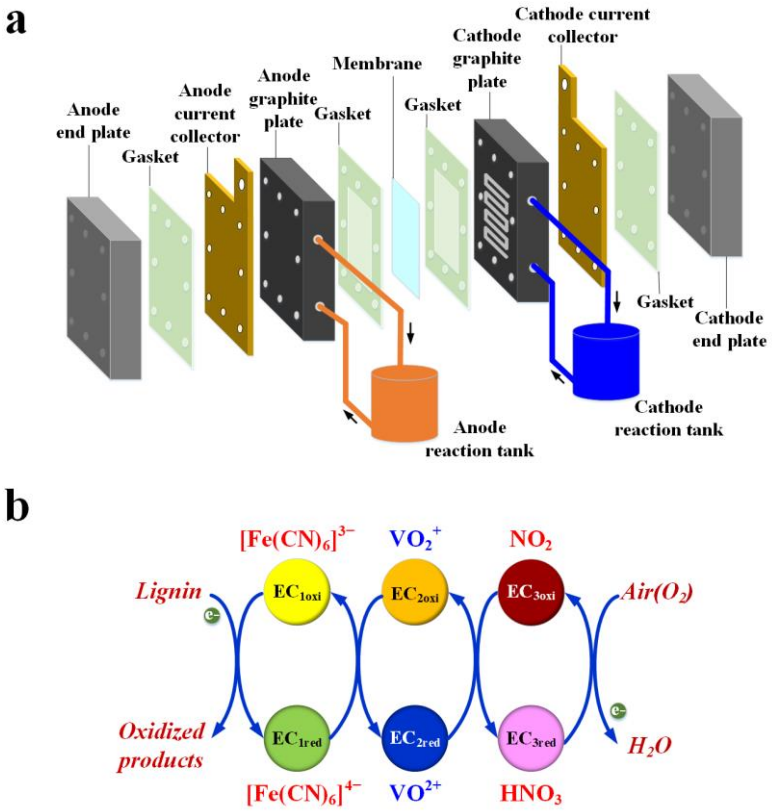

Fig. S10 Recovery and concentration of H_2O_2 from catholyte. (a) The process flow scheme designed in this work. (b) Flow scheme of Aspen plus simulation and (c) the heat duty of the main units.

a

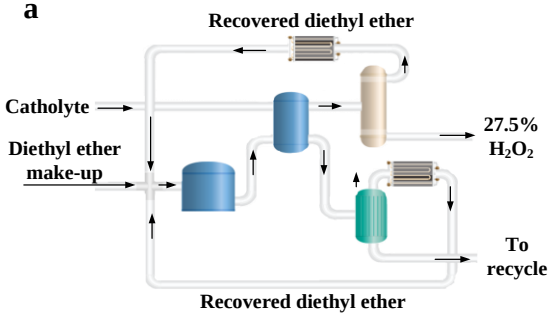

b

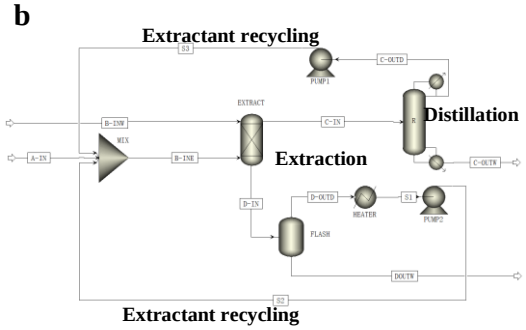

c

Unit	Heat duty (MW)
From neutral catholyte (water)	
Flash tank	0.048
Reboiler of rectification column	1.637
From alkaline catholyte (KOH solution)	
Flash tank	0.046
Reboiler of rectification column	1.690

Fig. S11 Effects of operation parameters on the recovery of H_2O_2 from neutral catholyte (water) by simulated extraction and distillation. (a) Effects of volume ratio of extractant and H_2O_2 solution (V_B/V_A) and stages of the extraction column on extraction rate of H_2O_2. (b) and (c) Effects of reflux ratio and mass ratio of distillate to feed (denoted as mass ratio of D:F) of the rectification column on mass fraction of H_2O_2 in the distillate. (d) Effects of mass ratio of D:F on gaseous and liquid temperature at the bottom of rectification column. (e) and (f) Effects of the temperature and pressure of flash tank on the recovery rate and mass fraction of the ether stream.

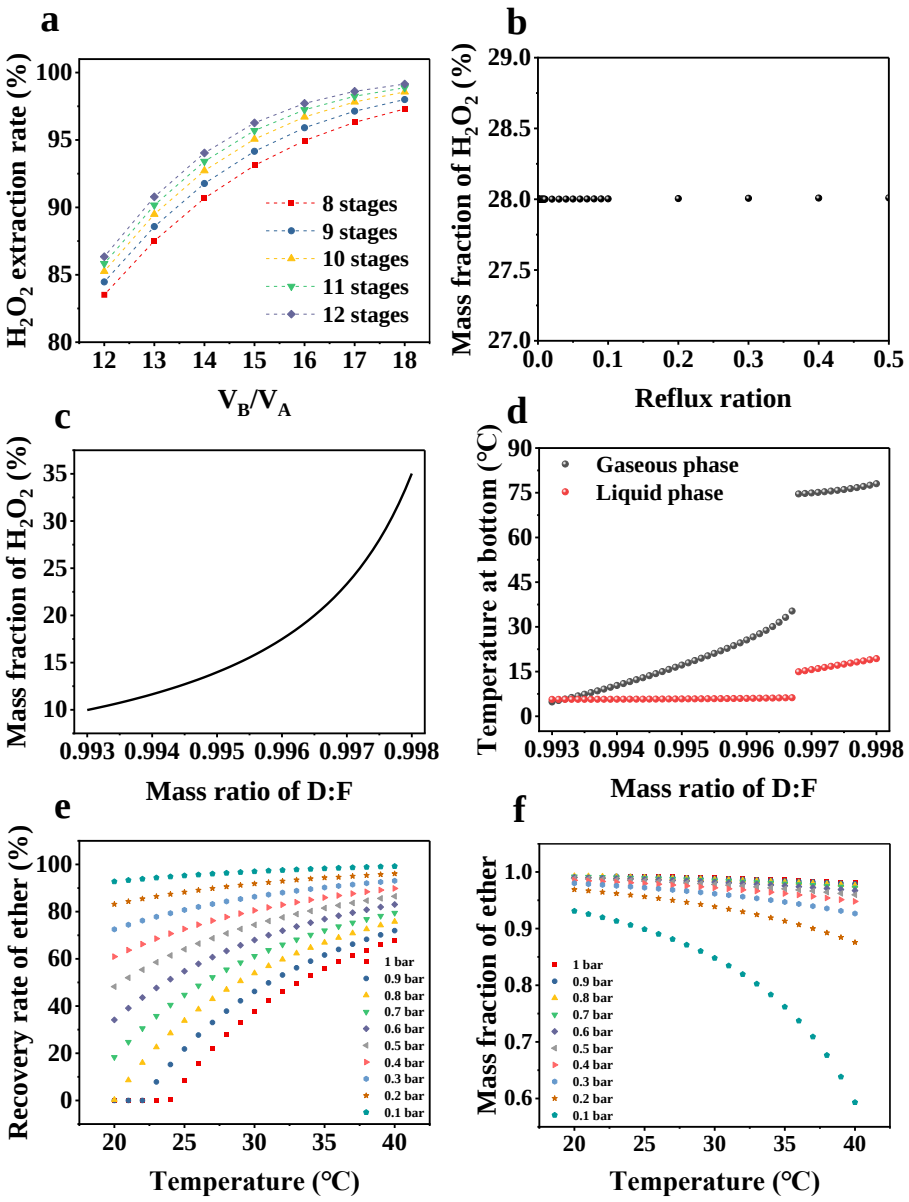

Fig. S12 Mass balance of extraction of H_2O_2 from (a) neutral electrolyte (water) and (b) alkaline electrolyte (KOH solution).

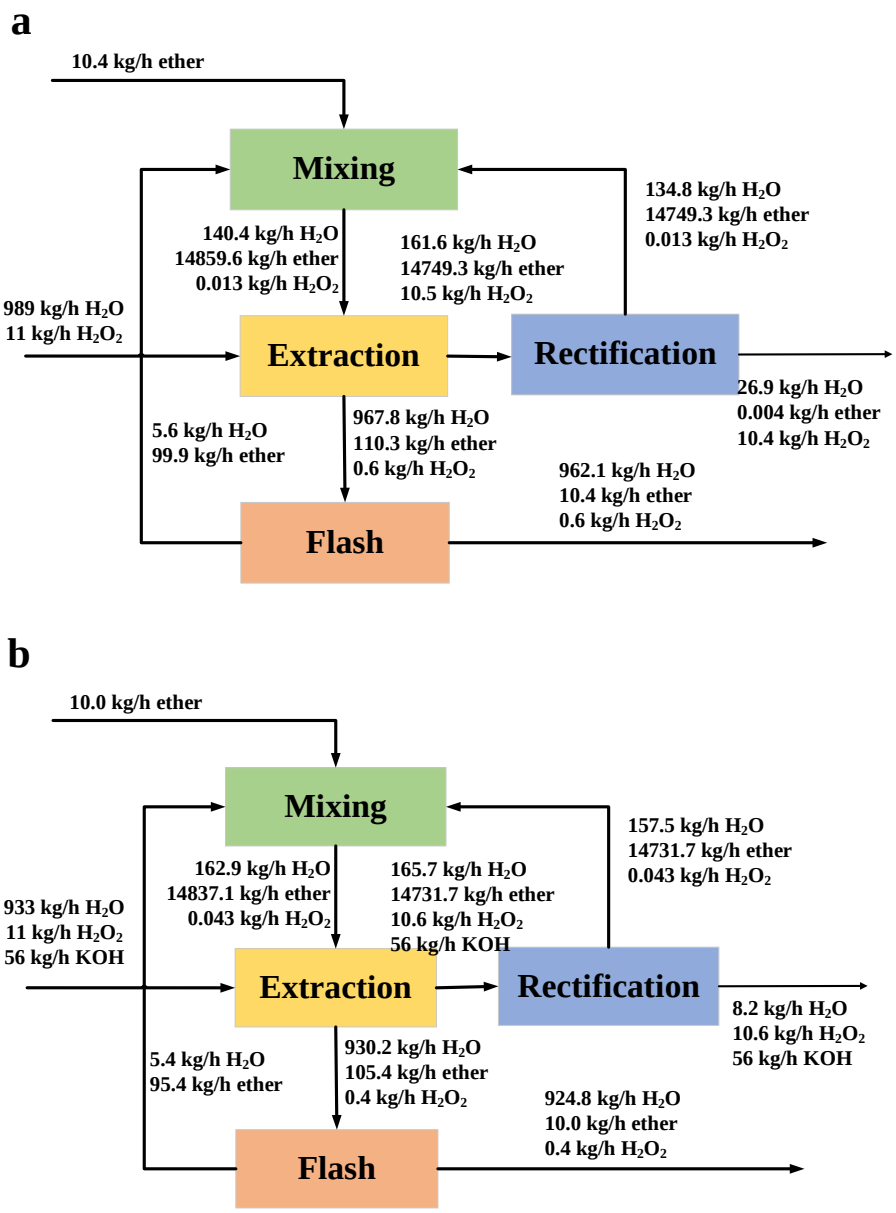

Fig. S13 In-situ use of H_2O_2 for oxidation of HMF. (a) Schematic diagram of oxidation of HMF to HMFCA using in-situ generated H_2O_2 as the oxidant agent. (b) HMF conversion and (c) HMFCA yield in non-electrolytic system, H-type cell and flow cell. (d) Proposed mechanism for the in-situ oxidation of HMF by H_2O_2 in Ag_2O catalytic system.

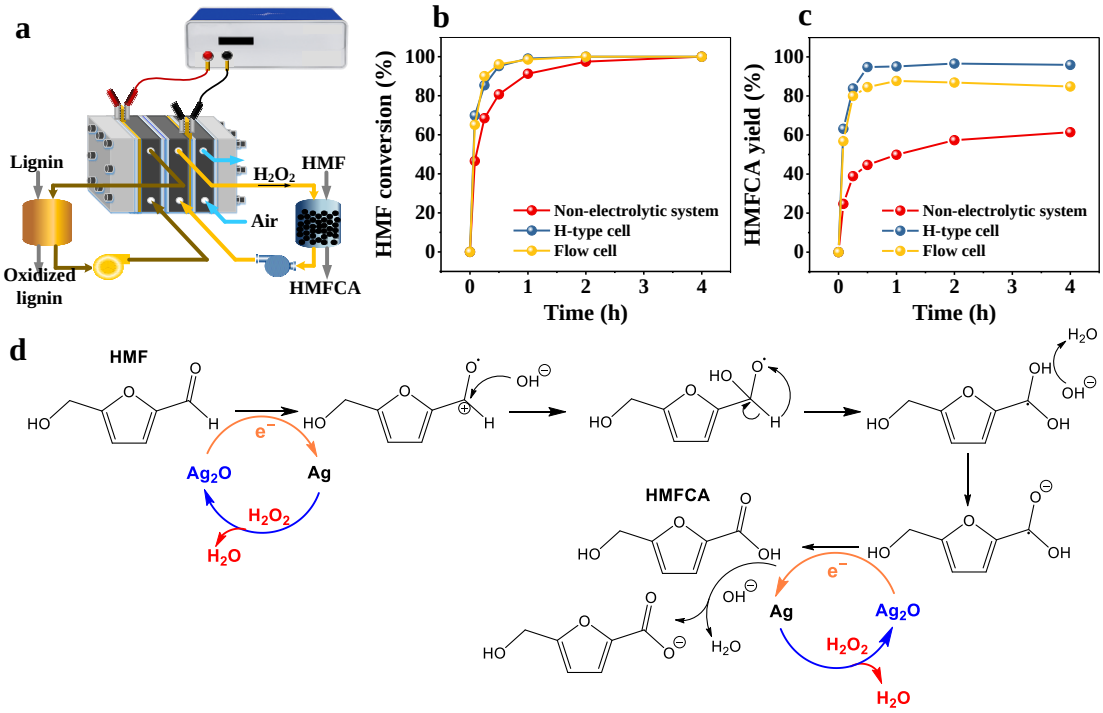

Table S1 Comparison on H_2O_2 productivity with recently reported results of different metal-free carbon-based catalysts in alkaline electrolyte

Material	Electrolyte	Productivity (mmol g_{cat}^{-1} h^{-1})	Catalyst loading (mg cm^{-2})	Applied potential (V vs. RHE)	Faradaic efficiency	Stability	Refs.
B-C-O900	0.1 M KOH	4122, 85% iR	1.0	0.56	95%	—	This work
	1 M KOH	4635, 0% iR	1.0	0.36	>98%	120 h @ 100 mA cm^{-2} in	This work
		11812 ,85% iR	1.0	0.56	95.7%	flow cell	This work
B doped C	1 M KOH	14.7, 100% iR	0.5	0.685	85.1%	30 h @ 200 mA cm^{-2} in flow cell	12
O-CNT	0.1 M KOH	~117	0.5	50 mA cm^{-2}, 0.5h	90%	10 h in RRDE	13
O, N doped carbon nanohorns	0.1 M KOH	740, 100% iR	0.5	0.65	50%	12 h @ 50 mA cm^{-2} in flow cell	14
B, N doped carbon nanosheets	0.1 M KOH	1787	0.25	−1.4 V	>80%	9 h @ 50 mA cm^{-2} in flow cell	15
N,O doped carbon nanotubes	1 M KOH	264.8	2	0.2, 10 mA cm^{-2}	95%	24 h in H cell	16
Honeycomb carbon nanofibers	0.1 M KOH	6.37 mmol L^{-1} h^{-1}	0.05	0.50	>89%	12 h in RRDE	17
N doped graphene oxide	0.1 M KOH	224.8	0.1	0.2	>43.6%	4 h in H cell	18
N doped ordered mesoporous carbon	0.1 M KOH	325	0.05	0.6	~99%	12 h @ 3 mA cm^{-2} in flow cell	19
Carbon black plasma	0.1 M KOH	300A/g	—	—	~100%	10 h in RRDE	20
Graphene-Like Nanocarbon	0.1 M KOH	355 mmol L^{-1} g^{-1} h^{-1}	0.5	0.1	~100%	3 h in H cell	21
Anthraquinone doped carbon nanotube	0.1 M NaOH	8.8	—	—	—	8 h in RRDE	22
Microwave treated CMK-3	0.1 M KOH	2476	0.1875	0.3	95%	8 h in H cell	23
O-BC	0.1 M KOH	412.8, 85% iR	0.2	0.5	74%	3 h in H cell	24
3D crumpled graphene	0.1 M KOH	473.9	0.8	0.4	92%	46 h @ 0.5 mA cm^{-2} in H	25

						cell	
W1/NO-C	0.1 M KOH	1230	0.2	0.2	95%	1 h in H cell	26
P, N doped carbon	0.1 M KOH	698.4	1	0.1	87%	12 h in RRDE, 4 h @ 3.4 mA cm^{-2} in H cell	27
N doped carbon	0.1 M KOH	1286.9	0.1	0.1	69.8%	—	28
N doped mesoporous carbon	0.1 M KOH	561.7	0.05	0.1	>70%	6 h in H cell	29
N, O doped carbon xerogel	0.1 M KOH	1410	0.1	—	78.3%	10 h in RRDE, 6 h @ 10 mA cm^{-2} in H cell	30
N-doped carbon (NPC) nanopolyhedra	1 M KOH	8740	0.2	100 mA cm^{-2}	~90%	200 h @ 100 mA cm^{-2} in flow cell	31
Vertical graphene edges	0.1 M KOH	1767	0.1	0.4	>80%	10 h in RRDE, 3 h @ 13 mA cm^{-2} in H cell	32
Ni2B	0.1 M KOH	4753	0.4	0.4	93%	12 h @ 125 mA cm^{-2} in flow cell	33
Defective porous carbons	0.1 M KOH	115.3	0.6	0.5	89%	12 h in RRDE, 3 h in full cell	34
PTFE@CNTs	0.1 M KOH	~10000	0.02	0.4	>95	6 h @ −0.2 V vs. RHE in H cell	35
N doped graphene/mesoporous carbon composite	0.1 M KOH	~7000	0.04	0.2	78	24 h @ 30 mA cm^{-2} in H cell	36
BS-C	0.1 M KOH	756	1	0.2	>90%	11 h @ 50 mA cm^{-2} in flow cell	37
B,F doped carbon nanotubes	0.1 M KOH	12500	0.007	0.17	90%	24 h @ 0.02 mA cm^{-2} in H cell	38
Framework interlaced COFs	0.1 M KOH	~5000	—	70 mA cm^{-2}	30%	20 h in RRDE	39

Imine-linked COF	0.1 M KOH	218	—	2 mA cm^{-2}	88%	16 h in RRDE, 10000 s @ 2 mA cm–2 in H cell	40
Commercial carbon black	0.1 M KOH with 10 mM DMSO	~6000	0.1	0.3	90%	10 h @ 0.3 V vs. RHE in H cell	41
N,B doped graphene quantum dots	0.1 M KOH	709	1	0.2	81%	12 h @ 50 mA cm^{-2} in flow cell	42

Table S2 Comparison on H_2O_2 productivity with recently reported results of different metal-based catalysts in alkaline electrolyte

Material	Electrolyte	Productivity (mmol g_{cat}^{-1} h^{-1})	Catalyst loading (mg cm^{-2})	Applied potential (V vs. RHE)	Faradaic efficiency	Stability	Ref.
B-C-O900	0.1 M KOH	4122, 85% iR	1.0	0.56	95%	—	This work
	1 M KOH	4635, 0% iR	1.0	0.36	>98%	120 h @ 100 mA cm^{-2} in	This work
		11812, 85% iR	1.0	0.56	95.7%	flow cell	This work
Co-O-C	0.1 M $KHCO_3$ + 0.05 M KNO_3	150	0.25	0.4	75.7	2 h in H cell	43
NiFe-MOFs	0.1 M KOH	1830	0.2	0.5	96.3	14 h @ 5 mA cm^{-2} in H cell	44
Oxygen-vacancy-enriched Bi_2O_3 nanorods	0.1 M KOH	~7500	0.2	100 mA cm^{-2}	69.9%	12 h @ 100 mA cm^{-2} in flow cell	45
Mn-NO-C_H	1 M KOH	~4000	0.16	0.5	~100%	55 h @ 0.1 V vs RHE in flow cell	46
Zn_2SnO_4/SnO_2	1 M KOH	~3000	0.0002	0.5	90%	12 h @ 100 mA cm^{-2} in flow cell	47
$BiOS_{SA}/Bi_{clu}$	0.1 M KOH	1458	0.121	0.5	50%	22 h @ 5 mA cm^{-2} in H cell	48
Co-N_5-O-C	1 M KOH	~6000	0.8	100 mA cm^{-2}	82.5%	24 h @ 100 mA cm^{-2} in flow cell	49

Table S3 Comparison of reported works on 2e-ORR pairing with other electrooxidation reactions.

Cathode (2e-ORR)			Anode			Stability tests of paired system	$\triangle E$ (V)[a]	Reduction in energy consumption (%)	Ref.
Catalyst	Productivity	FE (%)	Oxidation reaction	Catalyst or electron mediator	Productivity, FE				
B,O-C	~12 mmol L^{-1} h^{-1}	98	Lignin oxidative depolymerization	$[Fe(CN)_6]^{3-}$/ $[Fe(CN)_6]^{4-}$	—	10 h @ 67 mA cm^{-2}	–0.2	11.4 (by electrolysis)	This work
NiAl-LDH	2.92 mmol h^{-1} cm^{-2}	>90	Ethylene glycol to glycolic acid	Au/$Ni(OH)_2$	2.09 mmol h^{-1} cm^{-2}, >90% FE	10 h	—	5.8 (by electrolysis)	50
B/N-C	—	—	PET upcycling	Ni_1Mn_1-MOF-Se/NF	—	10 h @ ~50 mA cm^{-2}	–0.27	18.5 (by LSV)	51
Zn–N_2O_2	—	—	Polysulfides to sulfur powder	Zn–N_2O_2	—	16 h @ 10 mA cm^{-2}	–1.68	45 (by LSV)	52
TS-1@CoNC	—	47.74	Furfural to furoic acid	Ni foam	2.98% conversion, 93.35% FE	—	—	—	53
O-CNT	24 μmol min^{-1}	~90	WOR to H_2O_2	CFP-60%	~60% FE	2.5 h @ 120 mA cm^{-2}	—	—	54
O-CNT	56.1 μmol min^{-1}	75	WOR to H_2O_2	$Ni_{0.13}Ti_{0.87}O_{2-y}$	53.1 μmol min^{-1}, 71% FE	7 cycles	—	—	55

$\triangle E$: The difference in applied voltage between paired system and the conventional system.

References

1. F. Wang, D. Ouyang, B. Li, T. Liu and X. Zhao, *Energy Convers. Manag.*, 2022, **258**, 115552.
2. Y. Xia, X. Zhao, C. Xia, Z.-Y. Wu, P. Zhu, J. Y. Kim, X. Bai, G. Gao, Y. Hu, J. Zhong, Y. Liu and H. Wang, *Nat. Commun.*, 2021, **12**, 4225.
3. D. Ouyang, F. Wang, J. Hong, D. Gao and X. Zhao, *Appl. Energy*, 2021, **304**, 117927.
4. D. Ouyang, D. Gao, J. Hong, Z. Jiang and X. J. Zhao, *J. Energy Chem.*, 2023, **79**, 135-147.
5. D.-J. Chen, B. Xu, S.-G. Sun and Y. J. Tong, *Catal. Today*, 2012, **182**, 46-53.
6. S. Nayak, I. J. McPherson and K. A. Vincent, *Angew. Chem. Int. Ed.*, 2018, **57**, 12855-12858.
7. G. Kresse and D. Joubert, *Physical Review B*, 1999, **59**, 1758-1775.
8. J. P. Perdew, K. Burke and M. Ernzerhof, *Phys. Rev. Lett.*, 1996, **77**, 3865.
9. Z. Lu, G. Chen, S. Siahrostami, Z. Chen, K. Liu, J. Xie, L. Liao, T. Wu, D. Lin, Y. Liu, T. F. Jaramillo, J. K. Nørskov and Y. Cui, *Nat. Catal.*, 2018, **1**, 156-162.
10. G. Henkelman, A. Arnaldsson and H. Jónsson, *Comput. Mater. Sci*, 2006, **36**, 354-360.
11. J. K. Nørskov, J. Rossmeisl, A. Logadottir, L. Lindqvist, J. R. Kitchin, T. Bligaard and H. Jónsson, *The Journal of Physical Chemistry B*, 2004, **108**, 17886-17892.
12. Y. Xia, X. Zhao, C. Xia, Z.-Y. Wu, P. Zhu, J. Y. Kim, X. Bai, G. Gao, Y. Hu and J. Zhong, *Nat. Commun.*, 2021, **12**, 4225.
13. Z. Lu, G. Chen, S. Siahrostami, Z. Chen, K. Liu, J. Xie, L. Liao, T. Wu, D. Lin, Y. Liu and C. Yi, *Nat. Catal.*, 2018, **1**, 156-162.
14. P. Chakthranont, S. Nitrathorn, S. Thongratkaew, P. Khemthong, H. Nakajima, R. Supruangnet, T. Butburee, N. Sano and K. Faungnawakij, *ACS Appl. Energy Mater.*, 2021, **4**, 12436-12447.
15. Z. Tian, Q. Zhang, L. Thomsen, N. Gao, J. Pan, R. Daiyan, J. Yun, J. Brandt, N. López‐Salas and F. Lai, *Angew. Chem. Int. Ed. Engl.*, 2022, **134**, e202206915.
16. S. Xu, R. Lu, K. Sun, J. Tang, Y. Cen, L. Luo, Z. Wang, S. Tian and X. Sun, *Adv. Sci.*, 2022, **9**, 2201421.
17. K. Dong, J. Liang, Y. Wang, Z. Xu, Q. Liu, Y. Luo, T. Li, L. Li, X. Shi and A. M. Asiri, *Angew. Chem. Int. Ed. Engl.*, 2021, **60**, 10583-10587.
18. L. Han, Y. Sun, S. Li, C. Cheng, C. E. Halbig, P. Feicht, J. L. Hübner, P. Strasser and S. Eigler, *ACS Catal.*, 2019, **9**, 1283-1288.
19. B. S. Rawah, M. Albloushi and W. Li, *ACS Sustain. Chem. Eng.*, 2022, **10**, 5453-5462.
20. Z. Wang, Q.-K. Li, C. Zhang, Z. Cheng, W. Chen, E. A. McHugh, R. A. Carter,

B. I. Yakobson and J. M. Tour, *ACS Catal.*, 2021, **11**, 2454-2459.
21. C. Zhang, J. Zhang, J. Zhang, M. Song, X. Huang, W. Liu, M. Xiong, Y. Chen, S. Xia and H. Yang, *ACS Sustain. Chem. Eng.*, 2021, **9**, 9369-9375.
22. D. Wielend, M. Vera-Hidalgo, H. Seelajaroen, N. S. Sariciftci, E. M. Pérez and D. R. Whang, *ACS Appl. Mater. Interfaces*, 2020, **12**, 32615-32621.
23. Y.-L. Wang, S.-S. Li, X.-H. Yang, G.-Y. Xu, Z.-C. Zhu, P. Chen and S.-Q. Li, *J. Mater. Chem. A*, 2019, **7**, 21329-21337.
24. Y. Chang, J. Li, J. Ma, Y. Liu, R. Xing, Y. Wang and G. Zhang, *Sci. China Mater.*, 2022, **65**, 1276-1284.
25. K. Lee, J. Lim, M. J. Lee, K. Ryu, H. Lee, J. Y. Kim, H. Ju, H.-S. Cho, B.-H. Kim and M. C. Hatzell, *Energy Environ. Sci.*, 2022, **15**, 2858-2866.
26. F. Zhang, Y. Zhu, C. Tang, Y. Chen, B. Qian, Z. Hu, Y. C. Chang, C. W. Pao, Q. Lin and S. A. Kazemi, *Adv. Funct. Mater.*, 2022, **32**, 2110224.
27. Z. Li, A. Kumar, N. Liu, M. Cheng, C. Zhao, X. Meng, H. Li, Y. Zhang, Z. Liu and G. Zhang, *J. Mater. Chem. A*, 2022, **10**, 14355-14363.
28. J. Zhang, G. Zhang, S. Jin, Y. Zhou, Q. Ji, H. Lan, H. Liu and J. Qu, *Carbon*, 2020, **163**, 154-161.
29. Y. Sun, I. Sinev, W. Ju, A. Bergmann, S. r. Dresp, S. Kühl, C. Spöri, H. Schmies, H. Wang and D. Bernsmeier, *ACS Catal.*, 2018, **8**, 2844-2856.
30. S. Xu, Y. Gao, T. Liang, L. Zhang and B. Wang, *Chin Chem Lett*, 2022, **33**, 5152-5157.
31. P. Cao, X. Quan, K. Zhao, X. Zhao, S. Chen and H. Yu, *ACS Catal.*, 2021, **11**, 13797-13808.
32. D. Zhang, C. Tsounis, Z. Ma, D. Djaidiguna, N. M. Bedford, L. Thomsen, X. Lu, D. Chu, R. Amal and Z. Han, *Small*, 2022, **18**, 2105082.
33. J. Wu, M. Hou, Z. Chen, W. Hao, X. Pan, H. Yang, W. Cen, Y. Liu, H. Huang and P. W. Menezes, *Adv. Mater.*, 2022, **34**, 2202995.
34. A. Yu, G. Ma, L. Zhu, R. Zhang, Y. Li, S. Yang, H.-Y. Hsu, P. Peng and F.-F. Li, *Appl. Catal. B*, 2022, **307**, 121161.
35. W. Peng, J. Qiu, X. Liu, H. Tan, F. Hou, J. Feng, X. Yan and J. Liang, *Adv. Funct. Mater.*, 2024, **34**, 2411353.
36. W. Peng, J. Liu, X. Liu, L. Wang, L. Yin, H. Tan, F. Hou and J. Liang, *Nat. Commun.*, 2023, **14**, 4430.
37. Y. Wu, Q. Yuan, Y. Zhao, X. Xu, J. Xu, Y. Wang, K. Sun, A. Wang, H. Sun, B. Li, R. Xu, Z. Wang, J. Jiang and M. Fan, *ACS Sustainable Chem. Eng.*, 2023, **11**, 13363-13373.
38. B. Guo, Q. Jiang, Z. Mao, Y. Zeng, R. Chen, D. a. Yang, L. Yin, F. Hou and J. Liang, *Carbon*, 2024, **222**, 118997.
39. H. Wu, L. Li, H. Chen, Y. Xing, Z. Wang, C. Zhang and X. Long, *Angew. Chem. Int. Ed.*, 2024, **63**, e202410719.
40. S. Huang, B. Zhang, D. Wu, Y. Xu, H. Hu, F. Duan, H. Zhu, M. Du and S. Lu, *Appl. Catal. B: Environ.*, 2024, **340**, 123216.

41. Y. Fang, Y. Fan, K. Xie, W. Ge, Y. Zhu, Z. Qi, Z. Song, H. Jiang and C. Li, *Angew. Chem. Int. Ed.*, 2023, **62**, e202304413.
42. M. Fan, Z. Wang, K. Sun, A. Wang, Y. Zhao, Q. Yuan, R. Wang, J. Raj, J. Wu, J. Jiang and L. Wang, *Adv. Mater.*, 2023, **35**, 2209086.
43. S. Zhang, M. Jin, H. Xu, X. Zhang, T. Shi, Y. Ye, Y. Lin, L. Zheng, G. Wang, Y. Zhang, H. Yin, H. Zhang and H. Zhao, *Energy Environ. Sci.*, 2024, **17**, 1950-1960.
44. H.-T. Tang, Z.-J. Tang, R.-L. Li, L. Tian, R. Wang, S. Pu and Z.-Q. Liu, *Appl. Catal. B: Environ. Energy*, 2024, **358**, 124436.
45. Q. Zhang, C. Cao, S. Zhou, W. Wei, X. Chen, R. Xu, X.-T. Wu and Q.-L. Zhu, *Adv. Mater.*, 2024, **36**, 2408341.
46. L.-Y. Dong, J.-S. Wang, T.-Y. Li, T. Wu, X. Hu, Y.-T. Wu, M.-Y. Zhu, G.-P. Hao and A.-H. Lu, *Angew. Chem. Int. Ed.*, 2024, **63**, e202317660.
47. Y. Yang, A. Xu, Y. Ren, K. Li, K. Nie, Y. Huang, H. He, J. Xu and X. Yin, *Appl. Catal. B: Environ. Energy*, 2025, **361**, 124625.
48. P. Zhu, W. Feng, D. Zhao, P. Song, M. Li, X. Tan, T. Liu, S. Liu, W. Zhu, Z. Zhuang, J. Zhang and C. Chen, *Angew. Chem. Int. Ed.*, 2023, **62**, e202304488.
49. W. Zhang, J. W. Choi, S. Kim, T. T. Le, S. Nandy, C.-K. Hwang, S. Y. Paek, A. Byeon, K. H. Chae, S. Y. Lee, S. H. Kim, H. Song, J. Kim, J. Oh, J. W. Lee, S. S. Han and J. M. Kim, *Appl. Catal. B: Environ.*, 2023, **331**, 122712.
50. Y. Sun, K. Fan, J. Li, L. Wang, Y. Yang, Z. Li, M. Shao and X. Duan, *Nat. Commun.*, 2024, **15**, 6098.
51. J. Qi, Y. Du, Q. Yang, N. Jiang, J. Li, Y. Ma, Y. Ma, X. Zhao and J. Qiu, *Nat. Commun.*, 2023, **14**, 6263.
52. C. Ma, J. Wang, X. Liu, N. Li, W. Liu, Y. Li, X. Fan and W. Peng, *ACS Catal.*, 2024, **14**, 16522-16531.
53. S. Wu, H. Zhang, X. Huang and Z. Wei, *Chem. Commun.*, 2022, **58**, 8942-8945.
54. C. Xia, S. Back, S. Ringe, K. Jiang, F. Chen, X. Sun, S. Siahrostami, K. Chan and H. Wang, *Nat. Catal.*, 2020, **3**, 125-134.
55. Z. Wang, X. Duan, M. G. Sendeku, W. Xu, S. Chen, B. Tian, W. Gao, F. Wang, Y. Kuang and X. Sun, *Chem Catal.*, 2023, **3**, 100672.